

Highlights

Adaptive Conditional Forest Sampling for Spectral Risk Optimisation under Decision-Dependent Uncertainty

Marcell T. Kurbucz

- Four-phase framework minimising spectral risk under endogenous uncertainty.
- GRF conditional sampling adapts to decision-induced distribution shifts.
- Two-stage oracle reranking eliminates surrogate misranking near the optimum.
- Antithetic variates and CRN yield low-variance local refinement.
- Smallest cross-replication SD among all competitors across all six settings.

Adaptive Conditional Forest Sampling for Spectral Risk Optimisation under Decision-Dependent Uncertainty[★]

Marcell T. Kurbucz^{a,*,1}

^a*Institute for Global Prosperity, The Bartlett, University College London, 9–11 Endsleigh Gardens, London, WC1H 0EH, United Kingdom*

ARTICLE INFO

Keywords:

Spectral risk optimisation
Conditional Value-at-Risk
Decision-dependent uncertainty
Simulation optimisation
Generalised random forests

ABSTRACT

Minimising a spectral risk objective, defined as a convex combination of expected cost and Conditional Value-at-Risk (CVaR), is challenging when the uncertainty distribution is decision-dependent, making both surrogate modelling and simulation-based ranking sensitive to tail estimation error. We propose Adaptive Conditional Forest Sampling (ACFS), a four-phase simulation-optimisation framework that integrates Generalised Random Forests for decision-conditional distribution approximation, CEM-guided global exploration, rank-weighted focused augmentation, and surrogate-to-oracle two-stage reranking before multi-start gradient-based refinement. We evaluate ACFS on two structurally distinct data-generating processes: a decision-dependent Student-t copula and a Gaussian copula with log-normal marginals, across three penalty-weight configurations and 100 replications per setting. ACFS achieves the lowest median oracle spectral risk on the second benchmark in every configuration, with median gaps over GP-BO ranging from 6.0% to 20.0%. On the first benchmark, ACFS and GP-BO are statistically indistinguishable in median objective, but ACFS reduces cross-replication dispersion by approximately 1.8 to 1.9 times on the first benchmark and 1.7 to 2.0 times on the second, indicating materially improved run-to-run reliability. ACFS also outperforms CEM-SO, SGD-CVaR, and KDE-SO in nearly all settings, while ablation and sensitivity analyses support the contribution and robustness of the proposed design.

1. Introduction

Decision-making under uncertainty is a central problem in operations research, with stochastic programming providing an established modelling framework (Birge and Louveaux, 2011; Shapiro et al., 2021). A particularly challenging—yet increasingly relevant—class of problems arises when the distribution of uncertain parameters depends on the decision variable itself. This decision-dependent (or endogenous) uncertainty, whose modelling in stochastic programming was systematically developed by Goel and Grossmann (2006), appears naturally in demand-stimulated resource allocation, climate-sensitive infrastructure investment, and volume-dependent supply chain reliability (Apap and Grossmann, 2017; Hellemo et al., 2018). In such settings, a fixed Monte Carlo sample drawn independently of x is accurate only locally and can misrepresent P_x elsewhere. The static i.i.d. premise underlying classical Sample Average Approximation (SAA) therefore no longer applies (Shapiro et al., 2021), and the resulting empirical objective can be systematically biased away from the true P_x -dependent risk (Cutler et al., 2024).

At the same time, modern risk management increasingly requires solutions that control exposure to extremes rather than merely optimise expected performance. The Conditional Value-at-Risk (CVaR) (Rockafellar and Uryasev, 2000; Acerbi and Tasche, 2002), combined linearly with expected cost into a spectral risk objective (Acerbi, 2002; Ruszczyński and Shapiro, 2006), provides a coherent and practically interpretable framework for tail-risk control. Optimising such an objective when P_x itself shifts with x places simultaneous demands on conditional distribution estimation, global search over a non-convex landscape, and accurate tail quantification. Small errors at the tail level can dominate the ranking of near-optimal candidates. Methods that address these needs in isolation therefore tend to perform poorly in combination: flexible learners may not be paired with stable optimisation, and strong optimisers may rely on surrogate assumptions that do not survive distributional endogeneity.

Data-driven prescriptive analytics has recently emerged as a productive bridge between predictive modelling and optimisation (Bertsimas and Kallus, 2020; Elmachtoub and Grigas, 2022; Sadana et al., 2025). Forest-based

[★]This research did not receive any specific grant from funding agencies in the public, commercial, or not-for-profit sectors.

*Corresponding author

✉ m.kurbucz@ucl.ac.uk (M.T. Kurbucz)

ORCID(s): 0000-0002-0121-6781 (M.T. Kurbucz)

estimators—and Generalised Random Forests (GRF) in particular (Wager and Athey, 2018; Athey et al., 2019)—offer locally adaptive, weighted representations of conditional distributions: given a query x , the forest assigns observation weights reflecting local similarity in covariate space, producing an empirical approximation to P_x that improves with sample density. Several authors have leveraged data-driven surrogate approaches for simulation optimisation (Amaran et al., 2016; Kleijnen, 2018). However, most existing pipelines rely on a fixed global training set and do not adapt sampling density toward the regions that ultimately govern the optimum—precisely where conditional tail behaviour must be estimated accurately.

On the optimisation side, Bayesian Optimisation (BO) with Gaussian Process surrogates (Snoek et al., 2012; Shahriari et al., 2016; Frazier, 2018) is a widely used baseline for expensive black-box objectives. GP-based BO scales poorly beyond a few hundred evaluations and does not naturally accommodate decision-dependent distribution shifts, since the surrogate models the objective as a stationary process over x . The Cross-Entropy Method (CEM) (Rubinstein and Kroese, 2004; De Boer et al., 2005) provides an effective gradient-free alternative, but its tail-risk accuracy remains constrained by the Monte Carlo budget used per evaluation. Stochastic gradient methods for CVaR (Rockafellar and Uryasev, 2000) are appealing in principle, yet in practice they are sensitive to step-size schedules and finite-difference gradient noise, making them vulnerable to premature convergence in non-convex, heavy-tailed regimes. The growing intersection of machine learning and stochastic optimisation for contextual decision-making (Mandi et al., 2024; Sadana et al., 2025) highlights the need for algorithms that combine adaptive representation learning with robust global search; this need is particularly acute when the objective surface is shaped by endogenous distributional shifts.

The present paper makes seven contributions. We formulate spectral risk minimisation under decision-dependent heavy-tailed uncertainty and highlight why standard surrogate-based approaches can be ill-suited to this setting. We introduce ACFS, a four-phase algorithm that integrates GRF-based conditional weighted sampling, a CEM warm-start, Differential Evolution, and a direct data-generating-process quasi-Newton refinement. We propose a two-stage reranking mechanism that uses GRF for efficient shortlisting and then corrects the shortlist by direct-oracle rescoring, mitigating surrogate misrankings that can drive occasional solution-quality outliers. We implement antithetic variates through the copula together with CRN-consistent finite-difference gradients to obtain low-variance gradient estimates in the final refinement stage. We evaluate ACFS on two structurally distinct DGPs—a Student- t copula with decision-dependent marginals (DGP1) and a Gaussian copula with log-normal marginals designed to mimic supply-chain demand processes (DGP2)—across three penalty-weight configurations ($\lambda \in \{0.50, 0.70, 0.90\}$, $\alpha = 0.95, 100$ replications per setting). We conduct a component ablation study identifying the contribution of each algorithmic phase and present a hyperparameter sensitivity analysis characterising robustness over four influential parameters. All methods are implemented under comparable evaluation protocols to support fair comparison.

The remainder of the paper is organised as follows. Section 2 presents the problem formulation, the conditional weighted forest sampler, and the ACFS pipeline. Section 3 describes the competitor methods. Section 4 specifies both benchmarks and the experimental protocol. Section 5 reports and interprets the comparative, ablation, and sensitivity results. Section 6 concludes.

2. Methodology

2.1. Problem Formulation

Let $\mathcal{X} \subset \mathbb{R}^{d_x}$ be a compact feasible set and $(\Omega, \mathcal{F}, \mathbb{P})$ a probability space. For each decision $x \in \mathcal{X}$, let P_x denote a Borel probability measure on \mathbb{R}^{d_w} so that the uncertain parameter vector $W \in \mathbb{R}^{d_w}$ follows a distribution that may depend on x . Given a measurable cost function $C : \mathbb{R}^{d_w} \times \mathcal{X} \rightarrow \mathbb{R}$ and parameters $\lambda \geq 0$, $\alpha \in (0, 1)$, the spectral risk objective is:

$$J(x) = \mathbb{E}_{W \sim P_x}[C(W, x)] + \lambda \cdot \text{CVaR}_\alpha(C(W, x)), \quad (1)$$

where CVaR at confidence level α is given by the Rockafellar–Uryasev representation (Rockafellar and Uryasev, 2000):

$$\text{CVaR}_\alpha(Z) = \inf_{\tau \in \mathbb{R}} \left\{ \tau + \frac{1}{1-\alpha} \mathbb{E}[\max(Z - \tau, 0)] \right\}. \quad (2)$$

This formulation defines a coherent risk measure (Acerbi and Tasche, 2002) and leads to the optimisation problem:

$$x^* \in \arg \min_{x \in \mathcal{X}} J(x). \quad (3)$$

We assume oracle access: for any x , one can draw $W \sim P_x$ by simulation or experiment, while the analytic form of P_x is unknown. The goal is to solve (3) under a fixed total oracle budget. Because P_x shifts with x , a fixed pre-drawn sample cannot simultaneously represent P_x accurately across multiple candidate decisions, and surrogate constructions that ignore this shift can become systematically optimistic in directions where P_x concentrates tail mass.

2.2. Conditional Weighted Forest Sampling

The CWFS mechanism approximates P_x using a training dataset $\mathcal{D}_N = \{(x_i, W_i)\}_{i=1}^N$ with $W_i \sim P_{x_i}$. A d_W -component GRF (Athey et al., 2019) is fitted to \mathcal{D}_N ; for any query x it yields weights $w(x) = (w_1(x), \dots, w_N(x)) \in \Delta_N$:

$$w_i(x) = \frac{1}{K} \sum_{k=1}^K \frac{\mathbf{1}[x_i \in \ell_k(x)]}{|\ell_k(x)|}, \quad (4)$$

where K is the number of trees and $\ell_k(x)$ is the leaf containing x in tree k . A synthetic draw from the CWFS approximation is:

$$\tilde{W}_j = W_{I_j} + h \odot Z_j, \quad I_j \sim w(x), \quad Z_j \sim \mathcal{N}(0, I_{d_W}), \quad (5)$$

where $h = (h_1, \dots, h_{d_W})$ is a component-wise bandwidth derived from Silverman’s rule (Silverman, 1986) scaled by a tuning constant, and \odot denotes elementwise multiplication. Systematic resampling (Douc and Cappé, 2005) replaces independent multinomial draws to reduce variance. The Monte Carlo estimator of $J(x)$ based on n CWFS draws is denoted $\hat{J}_n(x)$.

2.3. The Four-Phase ACFS Algorithm

ACFS decomposes optimisation into four phases, with computational effort allocated according to the value of information at each stage. The algorithm begins by generating an initial training set \mathcal{D}_A of $N_A = 1,200$ points using a maximin Latin Hypercube Design (LHD) (McKay et al., 1979) over \mathcal{X} , collecting oracle draws $W_i \sim P_{x_i}$, and fitting a GRF to obtain the conditional weighted sampler \hat{P}_x^A . Before Differential Evolution, ACFS runs a Cross-Entropy warm-start (Rubinstein and Kroese, 2004) consisting of seven iterations with a population of 35 candidates, each evaluated with 300 Monte Carlo draws from the true DGP. The resulting mean μ_{CEM} localises a plausible basin and seeds one-third of the DE population via draws from $\mathcal{N}(\mu_{\text{CEM}}, 0.04^2 I)$. Differential Evolution (Price et al., 2005; Storn and Price, 1997) then minimises a fast KDE-based surrogate $\hat{J}_{\text{KDE}}(x)$ using $n_c = 100$ draws per evaluation, with a DE/current-to-best/1/bin strategy for 55 iterations at population size 85. At convergence, the final population is re-evaluated with the GRF surrogate at $n_f = 800$ draws to identify the top $K = 4$ elite candidates \mathcal{E} .

The second phase performs focused augmentation around these elites. For each $x^{(k)} \in \mathcal{E}$, perturbation points are generated by adding Gaussian noise ($\sigma = 0.025$) and projecting onto \mathcal{X} . The augmentation budget $N_B = 700$ is allocated by geometrically decaying rank weights (approximately 46%, 28%, 17%, 10%), concentrating sampling density near the most promising basins. The GRF is retrained on $\mathcal{D}_{AB} = \mathcal{D}_A \cup \mathcal{D}_B$ (1,900 points).

The third phase applies a two-stage reranking to a candidate pool of approximately 151 points drawn from the DE elites, a global LHC safety net, and the CEM basin. Stage 1 evaluates all candidates using the GRF surrogate at $n_f = 800$ draws and retains the top 60; Stage 2 evaluates those 60 directly under the true DGP with $n_d = 450$ samples each, selecting the top 30 seeds for local refinement. This targeted oracle correction eliminates outliers induced by surrogate ranking errors near the optimum at a small fraction of the cost of a full direct search.

The fourth phase refines the top 30 seeds using multi-start L-BFGS-B (Zhu et al., 1997) with direct DGP calls. Objective evaluations draw antithetic pairs $(Z, -Z)$ through the copula to generate $n_d = 450$ scenarios and cache the resulting W matrix; gradient evaluations reuse the same matrix via Common Random Numbers, producing central-difference gradients with negligible stochastic noise. The 30 local runs are fast (typically 15–25 effective iterations each) and complete in approximately 2–4 seconds in the benchmark environment.

Table 1

Pseudocode for the ACFS algorithm.

Input	\mathcal{X} , oracle simulator $W \sim P_x$, cost function C , budgets N_A, N_B
Output	$x^* \in \mathcal{X}$, an approximate minimiser of $J(x)$
Phase 1: Global exploration	
1	Generate LHD $\{x_i\}_{i=1}^{N_A}$, draw $W_i \sim P_{x_i}$; fit GRF on D_A
2	Run CEM warm-start (7 iter \times 35 pop \times 300 MC) $\rightarrow \mu_{\text{CEM}}$
3	Initialise DE: $\approx 33\%$ from $\mathcal{N}(\mu_{\text{CEM}}, 0.04^2 I)$, remainder LHC
4	Run DE on KDE surrogate ($n_c = 100$) for 55 iterations, population 85
5	Re-rank final DE population with GRF ($n_f = 800$); select top- $K = 4$ elites \mathcal{E}
Phase 2: Focused augmentation	
6	Geometrically weighted $N_B = 700$ augmentation draws around the elites
7	Retrain GRF on $D_{AB} = D_A \cup D_B$
Phase 3: Two-stage reranking	
8	Pool ≈ 151 candidates from elites, LHC safety net, and CEM basin
9	Stage 1: GRF scores all ($n_f = 800$) \rightarrow shortlist top 60
10	Stage 2: direct-DGP ($n_d = 450$) rescoring \rightarrow top 30 seeds
Phase 4: Direct-DGP L-BFGS-B	
11	For each seed: L-BFGS-B with antithetic $\text{fn}(x)$ and CRN-consistent $\text{gr}(x)$ (maxit = 80)
12	Return $x^* = \arg \min_{\text{starts}} \text{fn}(x)$

2.4. Variance Reduction

Two variance-reduction devices are embedded in the direct-DGP evaluator used in Phases 3 and 4. Antithetic variates pair each batch of $n_d/2$ standard-normal draws Z with $-Z$, map both through the decision-dependent correlation structure, and apply component-wise marginal quantile transforms. When the cost is approximately monotone in relevant directions, this pairing induces negative covariance between outcomes and reduces the variance of \hat{J} without additional oracle calls (Glasserman, 2004). Common Random Numbers reuse the same cached W matrix for objective and gradient evaluation at each L-BFGS-B iterate. Since $C(W, x)$ is deterministic in x for fixed W , the resulting central-difference gradients exhibit negligible stochastic noise, turning local refinement into a low-variance procedure (L’Ecuyer, 1994; Glasserman, 2004).

3. Competitor Methods

We benchmark ACFS against four representative methods. GP-BO fits a Gaussian Process with a squared-exponential ARD kernel, optimises hyperparameters by marginal log-likelihood, and uses Expected Improvement for sequential acquisition (Shahriari et al., 2016; Frazier, 2018). Starting from $n_{\text{init}} = 18$ LHC points, it performs 25 EI-guided evaluations (130 MC draws each), refits every five steps, and polishes the best observed point with L-BFGS-B. CEM-SO follows Rubinstein and Kroese (2004) with $T = 12$ iterations, population 55, elite fraction 15%, smoothing 0.60, and 130 MC draws per evaluation, followed by an L-BFGS-B polish at 4 \times the MC budget. SGD-CVaR applies Adam (Kingma and Ba, 2015) with a decaying learning rate and finite-difference gradients using mini-batches of 60 scenarios; two 80-iteration warm-start chains are followed by a 160-iteration fine search from the best warm start and an L-BFGS-B polish. KDE-SO trains a decision-weighted Gaussian KDE on 2,600 LHC points and minimises the surrogate using DE (100 KDE MC per evaluation), followed by multi-start L-BFGS-B from the best DE population members.

4. Computational Experiments

4.1. Benchmark Instances

4.1.1. DGPI: Student- t Copula with Decision-Dependent Marginals

We construct a six-dimensional synthetic benchmark with a five-variate decision-dependent uncertain parameter to expose the key challenges of spectral risk optimisation under heavy-tailed endogenous uncertainty. The decision vector $x = (x_1, \dots, x_5, x_6) \in \mathcal{X}$ satisfies $x_j \in [0, 0.70]$ for $j = 1, \dots, 5$, $x_6 \in [0, 1]$, and $\sum_{j=1}^5 x_j \leq 0.85$, with residual allocation $x_0 = \max(0, 1 - \sum_{j=1}^5 x_j)$. The uncertain parameter $W = (W_1, \dots, W_5)^\top$ follows a Student- t copula with decision-dependent marginal means $\mu(x)$, standard deviations $\sigma(x)$, degrees of freedom $\nu(x)$, and correlation matrix $R(x)$. To generate a sample, one draws a correlated normal $Z \sim \mathcal{N}(0, R(x))$, maps to uniforms via the standard normal

CDF, and applies component-wise Student- t quantile transforms. The full DGP specification is given in Table 2; mean, dispersion, tail weight, and cross-sectional dependence all shift nonlinearly with the decision, producing a genuinely endogenous distributional structure.

Table 2

Decision-dependent parameters of DGP1 (Student- t copula). $x_0 = \max(0, 1 - \sum_{j=1}^5 x_j)$; x_6 is the sixth decision variable.

Parameter	Expression	
$\mu_1(x)$	$2.10 - 1.50 x_6 - 1.10 x_1 + 1.20 x_0 + 0.75 x_2 x_3 - 0.55 x_1 x_6^2$	
$\mu_2(x)$	$2.30 - 1.30 x_1 - 1.70 x_3 + 0.95 x_0 - 0.65 x_6^2 + 0.45 x_2^2$	
$\mu_3(x)$	$1.90 - 1.50 x_2 - 1.05 x_6 + 0.75 x_0 + 0.55 x_1 x_2 - 0.35 x_3 x_6$	
$\mu_4(x)$	$1.70 - 1.20 x_4 - 0.90 x_6 + 0.60 x_0 + 0.40 x_3 x_5 - 0.30 x_2 x_4$	
$\mu_5(x)$	$1.50 - 1.00 x_5 - 0.80 x_6 + 0.50 x_0 + 0.35 x_1 x_4 - 0.25 x_3^2$	
$\sigma_1(x)$	$0.20 + 0.75(1 - x_6)(1 - x_1) + 0.30 x_0$	
$\sigma_2(x)$	$0.24 + 0.65(1 - x_3) + 0.28(1 - x_6) + 0.22 x_0$	
$\sigma_3(x)$	$0.22 + 0.60(1 - x_2) + 0.20(1 - x_6) + 0.16 x_0$	
$\sigma_4(x)$	$0.18 + 0.50(1 - x_4) + 0.18(1 - x_6) + 0.14 x_0$	
$\sigma_5(x)$	$0.16 + 0.45(1 - x_5) + 0.15(1 - x_6) + 0.12 x_0$	
$v_1(x)$	$3.0 + 2.5 x_6$	$v_2(x) = 3.0 + 2.0 x_3$
$v_3(x)$	$3.0 + 1.5 x_2$	$v_4(x) = 3.5 + 2.0 x_4$
$v_5(x)$	$3.5 + 1.5 x_5$	
$R_{12}(x)$	$0.55 + 0.28(1 - x_6)$	$R_{13}(x) = 0.20 + 0.28(1 - x_1)$
$R_{14}(x)$	$0.15 + 0.20(1 - x_2)$	$R_{15}(x) = 0.10 + 0.18(1 - x_3)$
$R_{23}(x)$	$0.50 + 0.32(1 - 2x_2)$	$R_{24}(x) = 0.20 + 0.22(1 - x_4)$
$R_{25}(x)$	$0.15 + 0.18(1 - x_5)$	$R_{34}(x) = 0.25 + 0.20(1 - x_3)$
$R_{35}(x)$	$0.18 + 0.16(1 - x_4)$	$R_{45}(x) = 0.30 + 0.25(1 - 2x_5)$

The cost function decomposes additively as:

$$C(W, x) = c_{\text{dmg}}(W, x) + c_{\text{hp}}(W, x) + c_{\text{ep}}(W, x) + c_{\text{del}}(W, x) + c_{\text{ac}}(x). \quad (6)$$

The benchmark is intentionally nonlinear: neither mean nor tail risk can be reduced by a single-variable adjustment, and the optimal allocation shifts with the spectral parameters λ and α .

4.1.2. DGP2: Gaussian Copula with Log-Normal Marginals

To assess the generalisability of ACFS beyond the Student- t setting, we introduce a second data-generating process with a qualitatively different distributional structure. DGP2 replaces the Student- t copula with a Gaussian copula and the symmetric scaled- t marginals with log-normal marginals, producing right-skewed, strictly positive uncertain parameters that are characteristic of demand and supply processes in operations management applications.

Formally, $W = (W_1, \dots, W_5)^\top$ is generated as follows. A correlated normal vector $Z \sim \mathcal{N}(0, R(x))$ is drawn using a decision-dependent correlation matrix $R(x)$ with entries of the form $R_{jk}(x) = b_{jk} + c_{jk} f(x)$, mapped to uniforms via $U_j = \Phi(Z_j)$, and then inverted through component-wise log-normal quantile functions: $W_j = \text{LogNormal}^{-1}(U_j; \mu_j(x), \sigma_j(x))$, where $\mu_j(x)$ and $\sigma_j(x)$ are the location and scale parameters of the log-normal distribution for component j at decision x . Both $\mu_j(x)$ and $\sigma_j(x)$ depend nonlinearly on all decision components, so that increases in any x_k simultaneously shift the mean, dispersion, and cross-sectional dependence of demand. The cost function captures supply-chain economics:

$$C(W, x) = c_{\text{hold}}(W, x) + c_{\text{short}}(W, x) + c_{\text{proc}}(W, x) + c_{\text{coord}}(W, x) + c_{\text{setup}}(x), \quad (7)$$

where c_{hold} and c_{short} are holding and shortage costs governed by capacity thresholds that shift with x , c_{proc} is a nonlinear procurement cost, c_{coord} penalises coordination overhead proportional to the total allocation, and c_{setup} is a quadratic fixed cost. This supply-chain interpretation contrasts with DGP1's damage/penalty structure and exercises a different region of the input space, providing a meaningful generalisability test.

4.2. Experimental Protocol

Three penalty-weight configurations are evaluated on both DGPs, all with $\alpha = 0.95$: a low-penalty setting ($\lambda = 0.50$), a balanced setting ($\lambda = 0.70$, used as the primary benchmark), and a high-penalty setting ($\lambda = 0.90$). As λ increases,

the CVaR component receives progressively greater weight relative to expected cost. Each configuration uses $R = 100$ independent replications. Final oracle evaluation of any candidate x^* uses 2,000 direct draws from the true P_x , with 400 bootstrap replicates for confidence intervals. All experiments are implemented in R and run on a single CPU core; reported wall-clock times correspond to an Apple M4 Pro MacBook Pro with 24 GB RAM running macOS Sequoia 15.1.

Results are reported as medians, standard deviations, and inter-quartile ranges across replications. For all six settings, pairwise Wilcoxon signed-rank tests (Wilcoxon, 1945; Hollander et al., 2014) with one-sided alternative $H_1 : J_{\text{ACFS}} < J_{\text{competitor}}$ assess statistical significance, with Holm correction controlling the family-wise error rate across four comparisons per setting. Bootstrap confidence intervals (400 resamples) are reported for the median paired difference (ACFS minus competitor), and rank-biserial correlations r_{rb} serve as standardised effect sizes. Per-replication win rates complement the hypothesis tests. Table 3 summarises key hyperparameters.

Table 3

Key hyperparameters of all five methods.

Method	Parameter	Value
ACFS	Stage-A LHC size N_A	1,200
	Stage-B augmentation N_B	700
	Top- K elite centres	4
	Augmentation radius r	0.025
	GRF trees / min-node	70 / 15
	DE iterations / population	55 / 85
	Scan pool size	≈ 151
	n_f (GRF re-rank MC)	800
	Phase-4 starts / maxit	30 / 80
	n_d (direct-DGP MC)	450
GP-BO	Init points / BO steps	18 / 25
CEM-SO	Iterations / population	12 / 55
SGD-CVaR	Warm iters / Full iters	80 / 160
KDE-SO	Training points	2,600

5. Results and Discussion

5.1. Comparative Performance

Figure 1 visualises the distribution of oracle objectives across 100 replications for all five methods on both DGPs and all three penalty-weight configurations. Table 4 summarises the median oracle spectral risk J_{med} , cross-replication standard deviation J_{SD} , and relative median gap to ACFS for all 30 method–setting combinations; full distributional statistics including inter-quartile ranges and expected-cost components are provided in Table 7 (Appendix A).

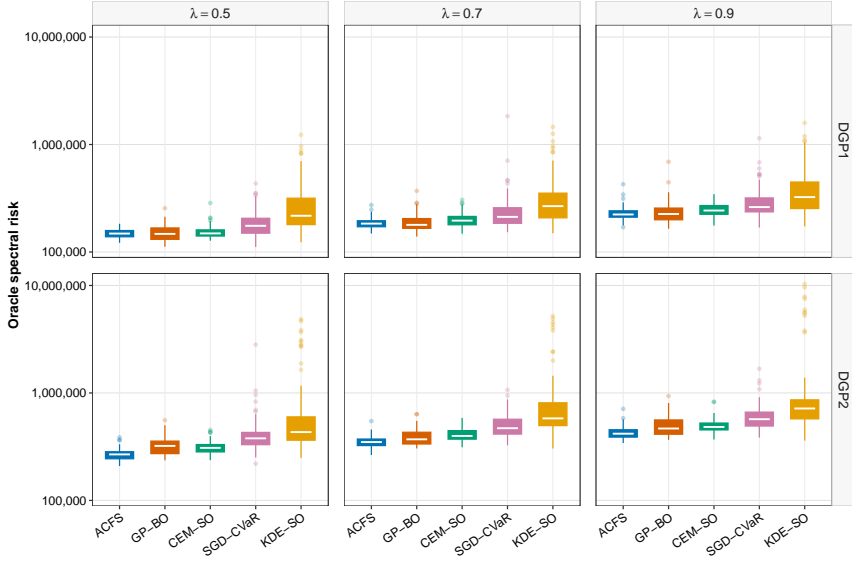


Figure 1: Oracle objective distributions across 100 replications for all five methods, both DGPs, and all three penalty-weight settings ($\lambda \in \{0.50, 0.70, 0.90\}$, $\alpha = 0.95$). Rows correspond to DGP1 (Student- t copula, top) and DGP2 (Gaussian copula with log-normal marginals, bottom); columns correspond to $\lambda = 0.50$, $\lambda = 0.70$, and $\lambda = 0.90$. The y -axis is shown on a logarithmic scale. ACFS exhibits a tighter distribution than GP-BO in every panel; the advantage is substantially larger on DGP2 where log-normal skewness amplifies tail estimation errors for GP-based surrogates.

Table 4

Comparative results summary. For each penalty weight λ , DGP1 and DGP2 results are shown side by side. Entries report median oracle spectral risk (J_{med}), cross-replication standard deviation (J_{SD}), and relative median gap to ACFS (Gap%). **Bold** denotes the lowest median within each DGP- λ block; *italics* mark GP-BO where it achieves a lower median than ACFS. A negative Gap% indicates the competitor achieves a lower marginal median.

λ	Method	DGP1			DGP2		
		J_{med}	J_{SD}	Gap%	J_{med}	J_{SD}	Gap%
0.50	ACFS	148,344	13,811	0.00	268,105	32,497	0.00
	<i>GP-BO</i>	147,284	25,438	-0.71	321,585	63,980	+19.95
	CEM-SO	148,872	22,634	+0.36	308,239	43,238	+14.97
	SGD-CVaR	175,178	57,814	+18.09	378,008	274,958	+40.99
	KDE-SO	217,294	198,869	+46.48	432,431	925,061	+61.29
0.70	ACFS	183,661	20,479	0.00	349,167	43,925	0.00
	<i>GP-BO</i>	178,842	38,294	-2.62	370,213	72,320	+6.03
	CEM-SO	195,800	32,179	+6.61	398,135	60,689	+14.02
	SGD-CVaR	212,139	178,980	+15.51	469,846	123,283	+34.56
	KDE-SO	266,973	237,362	+45.36	580,007	981,140	+66.11
0.90	ACFS	223,405	34,674	0.00	417,761	58,634	0.00
	GP-BO	225,628	65,961	+1.00	466,859	108,800	+11.75
	CEM-SO	243,081	34,714	+8.81	482,813	78,704	+15.57
	SGD-CVaR	261,606	127,013	+17.10	569,724	188,902	+36.38
	KDE-SO	324,096	257,886	+45.07	716,947	1,890,284	+71.62

Two consistent patterns emerge across both DGPs. On DGP1, ACFS and GP-BO form a clear top tier at every λ ; their marginal medians are close (within 2.62% at most), with GP-BO holding a slightly lower marginal median at $\lambda = 0.50$ and $\lambda = 0.70$ and ACFS marginally ahead at $\lambda = 0.90$. Despite this near-parity in central tendency, ACFS consistently exhibits substantially lower cross-replication dispersion: relative to GP-BO, the SD ratio ranges from 1.84 \times to 1.90 \times across the three DGP1 settings (J_{SD} : ACFS 13,811–34,674 versus GP-BO 25,438–65,961).

On DGP2, the picture shifts decisively in ACFS’s favour. ACFS achieves the lowest median in all three λ configurations, with gaps to GP-BO ranging from 6.0% ($\lambda = 0.70$) to 20.0% ($\lambda = 0.50$). The SD advantage is preserved: ACFS’s J_{SD} is 1.65 \times to 1.97 \times lower than GP-BO’s across DGP2 settings. This contrast between DGPs reflects the different demands each places on distributional approximation: under log-normal marginals, the objective landscape is more strongly right-skewed, making upper-tail estimation more delicate and ACFS’s GRF-based conditional sampling more decisive.

Across both DGPs and all λ values, CEM-SO, SGD-CVaR, and KDE-SO are uniformly dominated. The gap to KDE-SO exceeds 45% in every setting and reaches 71.6% on DGP2 at $\lambda = 0.90$, consistent with its sensitivity to decision-dependent distributional shifts. SGD-CVaR’s cross-replication SD is 3.7–5.4 \times larger than ACFS’s on DGP1 and 4.3–8.7 \times larger on DGP2, reflecting finite-difference gradient noise under heavy-tailed or right-skewed objectives. Runtime comparisons are consistent with the previous finding that CEM-SO is fastest (≈ 0.3 – 0.7 s); ACFS remains computationally competitive with GP-BO (both ≈ 4 – 7 s), while KDE-SO is consistently slower (≈ 7 – 15 s).

5.2. Statistical Significance

Table 5 reports paired Wilcoxon signed-rank tests for all six settings. Tests use 100 paired replication-level outcomes and are Holm-corrected within each setting. Negative median differences indicate lower oracle risk for ACFS.

Table 5

Paired Wilcoxon signed-rank tests for all six settings (H_1 : ACFS < competitor), Holm-corrected within each DGP– λ block. Median diff = ACFS–competitor (negative values favour ACFS); 95% CI is a bootstrap interval; r_{rb} is the rank-biserial effect size; Win% is the per-replication win rate of ACFS.

DGP	λ	Competitor	Med. diff	95% CI	p_{Holm}	r_{rb}	Win%
DGP1	0.50	GP-BO	+763	[−7,890; +8,146]	0.428 ns	0.021	48%
		CEM-SO	−2,729	[−9,227; +3,631]	0.152 ns	0.165	55%
		SGD-CVaR	−28,429	[−39,070; −21,381]	<0.001***	0.782	79%
		KDE-SO	−69,666	[−114,178; −50,584]	<0.001***	0.947	89%
	0.70	GP-BO	+1,332	[−4,043; +6,742]	0.490 ns	0.003	49%
		CEM-SO	−7,083	[−17,104; +64]	0.003**	0.346	60%
		SGD-CVaR	−31,001	[−40,892; −21,992]	<0.001***	0.695	76%
		KDE-SO	−77,770	[−109,891; −54,409]	<0.001***	0.917	87%
	0.90	GP-BO	+438	[−9,293; +11,240]	0.346 ns	0.046	50%
		CEM-SO	−15,450	[−25,415; −8,466]	<0.001***	0.381	67%
		SGD-CVaR	−40,506	[−59,850; −19,089]	<0.001***	0.710	77%
		KDE-SO	−82,131	[−120,304; −63,468]	<0.001***	0.894	86%
DGP2	0.50	GP-BO	−49,703	[−79,339; −36,746]	<0.001***	0.767	76%
		CEM-SO	−41,574	[−58,677; −26,165]	<0.001***	0.747	76%
		SGD-CVaR	−116,912	[−141,963; −94,727]	<0.001***	0.954	90%
		KDE-SO	−186,015	[−226,779; −151,853]	<0.001***	0.997	99%
	0.70	GP-BO	−44,083	[−61,563; −10,006]	<0.001***	0.485	64%
		CEM-SO	−58,396	[−81,854; −41,367]	<0.001***	0.773	81%
		SGD-CVaR	−127,607	[−155,278; −100,762]	<0.001***	0.965	92%
		KDE-SO	−244,978	[−298,211; −203,339]	<0.001***	0.983	94%
	0.90	GP-BO	−35,696	[−63,877; −24,444]	<0.001***	0.584	73%
		CEM-SO	−65,491	[−83,800; −46,282]	<0.001***	0.715	82%
		SGD-CVaR	−128,357	[−198,495; −105,373]	<0.001***	0.939	92%
		KDE-SO	−279,486	[−334,318; −236,455]	<0.001***	0.983	97%

The statistical picture reinforces the descriptive results. On DGP1, ACFS’s comparisons against GP-BO are non-significant after Holm correction at all three penalty levels ($p_{Holm} \geq 0.346$, $|r_{rb}| \leq 0.046$), confirming that the two methods are genuinely competitive on the Student- t benchmark. ACFS achieves statistically significant advantages over CEM-SO at $\lambda = 0.70$ and $\lambda = 0.90$ (both $p_{Holm} \leq 0.003$, r_{rb} 0.35–0.38), and large, highly significant advantages over SGD-CVaR and KDE-SO in every setting (all $p_{Holm} < 0.001$, $r_{rb} \geq 0.695$, win rates 76%–89%).

On DGP2, the results are uniformly strong. ACFS achieves statistically significant advantages over all four competitors in every λ configuration (all $p_{Holm} \leq 0.001$). Against GP-BO specifically, the effect sizes are moderate to large ($r_{rb} = 0.485$ – 0.767 , win rates 64%–76%), representing a qualitative shift relative to DGP1 where the two methods were indistinguishable. This contrast arises because GP-BO’s stationary process surrogate cannot adapt to the

asymmetric, right-skewed distributional shifts induced by log-normal marginals, while ACFS’s GRF-based conditional sampling tracks these shifts locally. The near-perfect win rates against KDE-SO on DGP2 (97%–99%) reflect the particular fragility of a global KDE surrogate under pronounced distributional endogeneity with heavy upper tails.

5.3. Mechanisms and Penalty-Weight Sensitivity

The DGP1 results illustrate a penalty-weight pattern that was already visible in the single-DGP analysis: ACFS’s advantage over GP-BO in central tendency is small on DGP1 and slightly reverses direction across λ without reaching statistical significance in any configuration. The most robust distinction is in dispersion, where ACFS’s SD advantage (1.84–1.90 \times) is preserved across all three settings. This suggests that the two-stage oracle reranking and antithetic variance reduction primarily operate by truncating the upper tail of the replication-level loss distribution rather than by achieving uniformly better median performance.

On DGP2, the mechanism through which ACFS outperforms is different: it captures the right-skewed conditional distribution more accurately at query points that are far from the training LHC design, where GP-BO’s global stationarity assumption leads to systematic underestimation of tail costs and hence misidentification of the optimal allocation. The GP-BO advantage visible on DGP1 at moderate λ therefore cannot be attributed to a general superiority of Bayesian optimisation, but to the specific matching between GP smoothness assumptions and the Student- t copula’s relatively symmetric marginal structure.

The expected-cost and CVaR components of the oracle objective reveal a qualitatively different mechanism on DGP2. On DGP2 at $\lambda = 0.70$, ACFS achieves a substantially lower median expected cost (55,830) than GP-BO (102,453), whereas GP-BO’s median CVaR (370,743) is lower than ACFS’s (419,115). ACFS and GP-BO are therefore finding structurally different solutions: ACFS identifies an allocation that minimises average cost at the expense of somewhat elevated tail risk, while GP-BO pursues a more risk-focused allocation that incurs substantially higher expected cost. At $\lambda = 0.70$, the spectral weighting favours ACFS’s solution; the advantage would likely narrow or reverse at very high λ where CVaR dominates the objective. On DGP1, the EC and CVaR components are broadly similar across methods, and differences in J are driven primarily by tail-estimation accuracy near the optimum rather than by qualitatively different solution strategies. This contrast further supports the view that GRF-based conditional sampling enables ACFS to find a cost-efficient region of the feasible set on the right-skewed DGP2 landscape that GP-BO’s stationary surrogate fails to identify.

5.4. Ablation Study

To isolate the contribution of each ACFS component, we evaluate four ablation variants on both DGPs at $\lambda = 0.70$ using 50 replications each. *ACFS-NoCEM* removes the CEM warm-start (Phase 1) and initialises DE purely from a Latin Hypercube sample. *ACFS-NoAug* removes the focused augmentation step (Phase 2), so the GRF trained on the initial $N_A = 1,200$ LHC points is used for all subsequent phases. *ACFS-NoRerank* removes Stage 2 direct-oracle rescoring (Phase 3), using GRF surrogate ranking alone to select the 30 L-BFGS-B starting points. *ACFS-NoAV* disables antithetic variates throughout, replacing the paired sampler with independent draws.

Table 6

Ablation study results ($\lambda = 0.70$, $\alpha = 0.95$, 50 replications). Gap% and σ -ratio are relative to ACFS-Full within each DGP. A σ -ratio below 1 indicates lower cross-replication SD than ACFS-Full; above 1 indicates higher SD. Wilcoxon p_{Holm} tests ACFS-Full vs. each variant; ns = not significant after Holm correction.

DGP	Variant	J_{med}	J_{SD}	Gap%	σ -ratio	p_{Holm}
DGP1	ACFS-Full	187,800	36,976	0.00	1.000	—
	ACFS-NoAV	189,221	23,287	+0.76	0.630	ns
	ACFS-NoCEM	192,843	21,344	+2.69	0.577	ns
	ACFS-NoRerank	193,799	32,001	+3.19	0.865	ns
	ACFS-NoAug	193,812	30,115	+3.20	0.814	ns
DGP2	ACFS-Full	340,077	35,714	0.00	1.000	—
	ACFS-NoAug	341,988	29,149	+0.56	0.816	ns
	ACFS-NoRerank	344,709	52,525	+1.36	1.471	ns
	ACFS-NoAV	347,635	45,046	+2.22	1.261	ns
	ACFS-NoCEM	353,671	42,265	+4.00	1.183	ns

ACFS-Full achieves the best median objective on both DGPs. The degradation from removing any single component ranges from 0.56% to 4.00%, with consistent ordering: NoCEM, NoAug, and NoRerank incur the largest penalties, while NoAV is generally the smallest contributor at the 50-replication scale. None of the pairwise differences reach statistical significance after Holm correction, reflecting the inherent variability at 50 replications—a limitation noted in the ablation design.

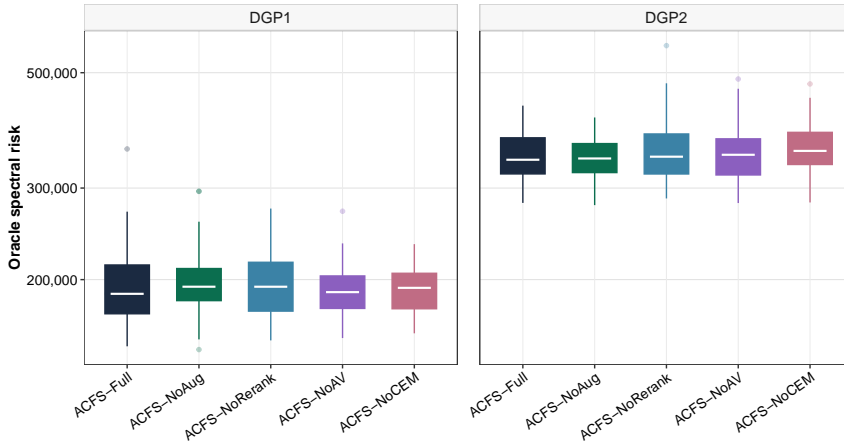


Figure 2: Ablation study results for DGP1 (left) and DGP2 (right) at $\lambda = 0.70$, $\alpha = 0.95$, 50 replications each. Each boxplot shows the distribution of oracle J across replications for one ACFS variant. The ordering of component importance differs between DGPs: removing the CEM warm-start incurs the largest penalty on DGP2 (right-skewed log-normal outcomes), while removing augmentation and two-stage reranking are jointly the most costly on DGP1.

The σ -ratio column reveals an interesting asymmetry. On DGP1, ACFS-Full has the highest SD of all five variants (σ -ratio ≤ 1 for all ablations), yet also the best median. This pattern is consistent with ACFS-Full conducting a broader search that occasionally identifies very good solutions (low J) and occasionally gets trapped in moderate-quality basins, whereas the ablation variants converge more reliably to mediocre solutions with lower variance but worse central tendency. On DGP2, this pattern reverses for NoRerank, NoAV, and NoCEM: all three have σ -ratios above 1 (1.471, 1.261, and 1.183 respectively), meaning their cross-replication SD exceeds ACFS-Full’s. The most pronounced effect is in NoRerank, where removing Stage-2 oracle rescoring inflates the SD to $1.47\times$ ACFS-Full’s level (from 35,714 to 52,525), indicating that under right-skewed log-normal marginals the oracle correction step specifically suppresses the high-cost outlier replications that are the primary driver of cross-replication variance. Only NoAug maintains a lower SD than ACFS-Full on DGP2 (ratio 0.816), suggesting that focused augmentation—while helpful for median quality—slightly increases tail dispersion on this benchmark.

5.5. Hyperparameter Sensitivity

We evaluate sensitivity over four key hyperparameters on DGP1 at $\lambda = 0.70$ using 20 replications per grid point. The parameters and grids are: training set size $N_A \in \{800, 1200, 1600\}$ (default 1,200); GRF re-rank MC draws $n_f \in \{400, 800, 1200\}$ (default 800); number of elite centres $K \in \{2, 4, 6\}$ (default 4); and direct-DGP MC draws $n_d \in \{300, 450, 600\}$ (default 450).

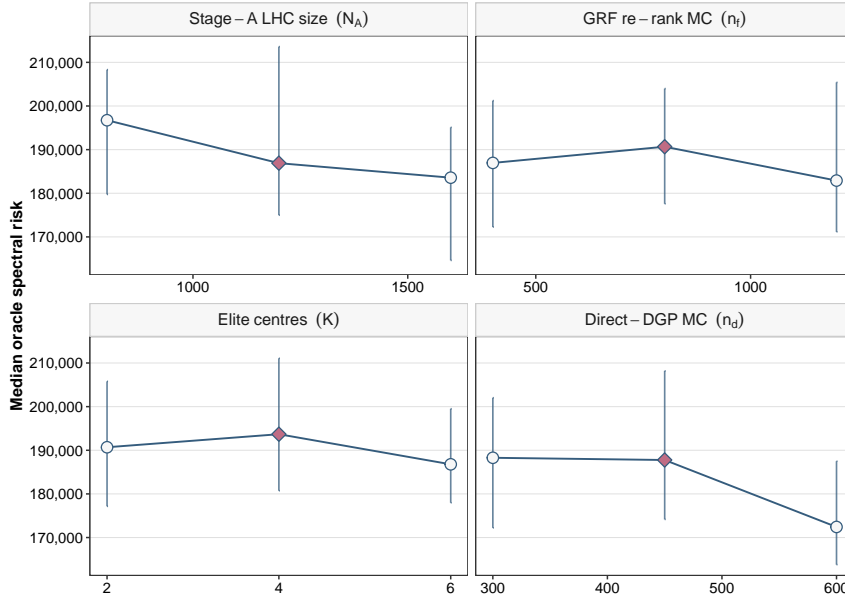


Figure 3: Hyperparameter sensitivity analysis on DGP1 at $\lambda = 0.70$, 20 replications per grid point. Each panel shows median oracle J (dots) and inter-quartile range (bars) as one parameter varies while others are held at their defaults. The dashed vertical line marks the default value used in the main experiments.

The results, displayed in Figure 3 and summarised in Table 8 (Appendix A), reveal a clear hierarchy of parameter importance. The direct-DGP MC budget n_d has the strongest and most consistent effect: increasing from the default $n_d = 450$ to $n_d = 600$ reduces the median objective from 187,773 to 172,427—an 8.2% improvement—suggesting that n_d is the most influential parameter in the tested range and that additional direct-oracle budget may further improve performance, albeit at additional computational cost. The training set size N_A shows a monotone positive effect: increasing from 800 to 1,600 reduces the median from 196,737 to 183,572, consistent with the expected improvement in GRF conditional estimation accuracy.

The GRF re-rank MC draws n_f and the number of elite centres K exhibit non-monotone patterns at 20 replications, with variation consistent with estimation noise at this grid size. The point estimates suggest that $n_f = 1200$ and $K = 6$ may be marginally beneficial relative to the defaults ($n_f = 800$, $K = 4$), but the differences are small and within the inter-quartile ranges, so no strong recommendation can be drawn from 20 replications. Overall, the algorithm shows reasonable robustness to parameter choice within the tested ranges, with the exception of n_d , which exhibits a consistent monotone trend across the grid.

6. Conclusions

We introduced ACFS, a four-phase data-driven algorithm for minimising a spectral risk objective under decision-dependent uncertainty. The method integrates GRF-based conditional sampling to represent distributional endogeneity, a CEM warm-start and Differential Evolution for global exploration, rank-weighted augmentation for local density improvement, and two-stage surrogate-to-oracle reranking to guard against tail-driven misranking near the optimum. The final refinement uses direct DGP calls with antithetic variates and CRN-consistent gradients to deliver fast, stable local convergence from multiple starts.

Evaluated on two structurally distinct benchmarks—a decision-dependent Student- t copula (DGP1) and a Gaussian copula with log-normal supply-chain marginals (DGP2)—across three penalty-weight configurations ($\lambda \in \{0.50, 0.70, 0.90\}$, $\alpha = 0.95$, 100 replications per setting), the results yield several consistent findings. On DGP1, ACFS and GP-BO are statistically indistinguishable in median oracle risk across all three λ values, while ACFS reduces cross-replication SD by 1.84–1.90 \times relative to GP-BO. On DGP2, ACFS achieves substantially lower medians in all configurations (gaps of 6.0%–20.0%, all $p_{\text{Holm}} < 0.001$), demonstrating that GRF-based conditional sampling captures asymmetric, log-normal-driven distributional shifts more effectively than GP surrogates. Against CEM-SO,

SGD-CVaR, and KDE-SO, ACFS achieves large and statistically significant advantages in nearly every setting on both DGPs.

The ablation study confirms that all four components—CEM warm-start, focused augmentation, two-stage oracle reranking, and antithetic variates—contribute positively to median performance (degradations of 0.56%–4.00% when each is removed), though differences are not individually significant at 50 replications. The sensitivity analysis identifies the direct-DGP MC budget n_d as the most influential parameter in the tested range: a 33% increase from the default $n_d = 450$ to $n_d = 600$ yields an 8.2% median improvement in this 20-replication study, suggesting a potential gain for higher-stakes deployments; the algorithm is broadly robust to variation in the remaining parameters within the tested ranges.

Future work includes extending ACFS to multi-fidelity and heterogeneous-cost simulators, developing adaptive schedules for the augmentation radius and warm-start MC budget based on observed surrogate accuracy, and improving scalability to $d_x \geq 20$ via sparse forest variants or dimensionality reduction. On the statistical side, replacing the current Stage-2 point-estimate oracle rescaling with a noise-aware selection rule—such as a variance-penalised criterion or a multi-sample average—could further suppress the high-cost outlier replications that remain the primary source of residual dispersion.

Declaration of Competing Interests

The author declares that there are no competing interests.

CRedit authorship contribution statement

Marcell T. Kurbucz: Conceptualization, Methodology, Software, Formal analysis, Writing – original draft, Writing – review & editing.

References

- Acerbi, C., 2002. Spectral measures of risk: a coherent representation of subjective risk aversion. *Journal of Banking & Finance* 26, 1505–1518. doi:10.1016/S0378-4266(02)00284-4.
- Acerbi, C., Tasche, D., 2002. On the coherence of expected shortfall. *Journal of Banking & Finance* 26, 1487–1503. doi:10.1016/S0378-4266(02)00283-2.
- Amaran, S., Sahinidis, N.V., Sharda, B., Bury, S.J., 2016. Simulation optimization: A review of algorithms and applications. *Annals of Operations Research* 240, 351–380. doi:10.1007/s10479-015-2019-x.
- Apap, R.M., Grossmann, I.E., 2017. Models and computational strategies for multistage stochastic programming under endogenous and exogenous uncertainties. *Computers & Chemical Engineering* 103, 233–274. doi:10.1016/j.compchemeng.2016.11.011.
- Athey, S., Tibshirani, J., Wager, S., 2019. Generalized random forests. *The Annals of Statistics* 47, 1148–1178. doi:10.1214/18-AOS1709.
- Bertsimas, D., Kallus, N., 2020. From predictive to prescriptive analytics. *Management Science* 66, 1025–1044. doi:10.1287/mnsc.2018.3253.
- Birge, J.R., Louveaux, F., 2011. *Introduction to Stochastic Programming*. 2nd ed., Springer, New York. doi:10.1007/978-1-4614-0237-4.
- Cutler, J., Diaz, M., Drusvyatskiy, D., 2024. Stochastic approximation with decision-dependent distributions: asymptotic normality and optimality. *Journal of Machine Learning Research* 25, 1–49.
- De Boer, P.T., Kroese, D.P., Mannor, S., Rubinstein, R.Y., 2005. A tutorial on the cross-entropy method. *Annals of operations research* 134, 19–67. doi:10.1007/s10479-005-5724-z.
- Douc, R., Cappé, O., 2005. Comparison of resampling schemes for particle filtering, in: *Proceedings of the 4th International Symposium on Image and Signal Processing and Analysis*, IEEE. pp. 64–69.
- Elmachtoub, A.N., Grigas, P., 2022. Smart “predict, then optimize”. *Management Science* 68, 9–26. doi:10.1287/mnsc.2020.3922.
- Frazier, P.I., 2018. A tutorial on bayesian optimization. arXiv preprint arXiv:1807.02811 URL: <https://arxiv.org/abs/1807.02811>.
- Glasserman, P., 2004. *Monte Carlo Methods in Financial Engineering*. volume 53 of *Stochastic Modelling and Applied Probability*. Springer, New York. doi:10.1007/978-0-387-21617-1.
- Goel, V., Grossmann, I.E., 2006. A class of stochastic programs with decision dependent uncertainty. *Mathematical Programming* 108, 355–394. doi:10.1007/s10107-006-0715-7.
- Hellemo, L., Barton, P.I., Tomaszgard, A., 2018. Decision-dependent probabilities in stochastic programs with recourse. *Computational Management Science* 15, 369–395. doi:10.1007/s10287-018-0330-0.
- Hollander, M., Wolfe, D.A., Chicken, E., 2014. *Nonparametric Statistical Methods*. 3rd ed., Wiley, Hoboken, NJ. doi:10.1002/9781119196037.
- Kingma, D.P., Ba, J., 2015. Adam: A method for stochastic optimization, in: *Proceedings of the 3rd International Conference on Learning Representations (ICLR)*. URL: <https://arxiv.org/abs/1412.6980>, doi:10.48550/arXiv.1412.6980.
- Kleijnen, J.P.C., 2018. *Design and Analysis of Simulation Experiments*. 3rd ed., Springer, Cham. doi:10.1007/978-3-319-76035-3.
- L’Ecuyer, P., 1994. Efficiency improvement and variance reduction, in: *Proceedings of the 1994 Winter Simulation Conference*, IEEE. pp. 122–132. doi:10.1109/WSC.1994.717089.

- Mandi, J., Kotary, J., Berden, S., Mulamba, M., Bucarey, V., Guns, T., Fioretto, F., 2024. Decision-focused learning: Foundations, state of the art, benchmark and future opportunities. *Journal of Artificial Intelligence Research* 80, 1623–1701. doi:[10.1613/jair.1.15320](https://doi.org/10.1613/jair.1.15320).
- McKay, M.D., Beckman, R.J., Conover, W.J., 1979. A comparison of three methods for selecting values of input variables in the analysis of output from a computer code. *Technometrics* 21, 239–245. doi:[10.1080/00401706.1979.10489755](https://doi.org/10.1080/00401706.1979.10489755).
- Price, K.V., Storn, R.M., Lampinen, J.A., 2005. *Differential Evolution: A Practical Approach to Global Optimization*. Springer, Berlin. doi:[10.1007/3-540-31306-0](https://doi.org/10.1007/3-540-31306-0).
- Rockafellar, R.T., Uryasev, S., 2000. Optimization of conditional value-at-risk. *Journal of Risk* 2, 21–42. doi:[10.21314/JOR.2000.038](https://doi.org/10.21314/JOR.2000.038).
- Rubinstein, R.Y., Kroese, D.P., 2004. The cross-entropy method: a unified approach to combinatorial optimization, Monte-Carlo simulation, and machine learning, volume 133. Springer. doi:[10.1007/978-1-4757-4321-0](https://doi.org/10.1007/978-1-4757-4321-0).
- Ruszczynski, A., Shapiro, A., 2006. Optimization of convex risk functions. *Mathematics of Operations Research* 31, 433–452. doi:[10.1287/moor.1050.0186](https://doi.org/10.1287/moor.1050.0186).
- Sadana, U., Chenreddy, A., Delage, E., Forel, A., Frejinger, E., Vidal, T., 2025. A survey of contextual optimization methods for decision-making under uncertainty. *European Journal of Operational Research* 320, 271–289. doi:[10.1016/j.ejor.2024.03.020](https://doi.org/10.1016/j.ejor.2024.03.020).
- Shahriari, B., Swersky, K., Wang, Z., Adams, R.P., de Freitas, N., 2016. Taking the human out of the loop: A review of Bayesian optimization. *Proceedings of the IEEE* 104, 148–175. doi:[10.1109/JPROC.2015.2494218](https://doi.org/10.1109/JPROC.2015.2494218).
- Shapiro, A., Dentcheva, D., Ruszczyński, A., 2021. *Lectures on Stochastic Programming: Modeling and Theory*. 3rd ed., Society for Industrial and Applied Mathematics, Philadelphia, PA. doi:[10.1137/1.9781611976595](https://doi.org/10.1137/1.9781611976595).
- Silverman, B.W., 1986. *Density Estimation for Statistics and Data Analysis*. Chapman & Hall, London.
- Snoek, J., Larochelle, H., Adams, R.P., 2012. Practical bayesian optimization of machine learning algorithms. *Advances in neural information processing systems* 25.
- Storn, R., Price, K., 1997. Differential evolution—A simple and efficient heuristic for global optimization over continuous spaces. *Journal of Global Optimization* 11, 341–359. doi:[10.1023/A:1008202821328](https://doi.org/10.1023/A:1008202821328).
- Wager, S., Athey, S., 2018. Estimation and inference of heterogeneous treatment effects using random forests. *Journal of the American Statistical Association* 113, 1228–1242. doi:[10.1080/01621459.2017.1319839](https://doi.org/10.1080/01621459.2017.1319839).
- Wilcoxon, F., 1945. Individual comparisons by ranking methods. *Biometrics Bulletin* 1, 80–83. doi:[10.2307/3001968](https://doi.org/10.2307/3001968).
- Zhu, C., Byrd, R.H., Lu, P., Nocedal, J., 1997. Algorithm 778: L-bfgs-b: Fortran subroutines for large-scale bound-constrained optimization. *ACM Transactions on mathematical software (TOMS)* 23, 550–560. doi:[10.1145/279232.279236](https://doi.org/10.1145/279232.279236).

A. Full Results Tables

Table 7 reports complete distributional statistics for all 30 method–setting combinations. Table 8 summarises the sensitivity analysis grid.

Table 7

Full oracle spectral risk statistics for all six settings ($\alpha = 0.95$, 100 replications). For each method and setting: median oracle spectral risk (J_{med}), standard deviation (J_{SD}), 25th and 75th percentiles ($J_{Q_{25}}$, $J_{Q_{75}}$), median expected cost (EC_{med}), and relative median gap to ACFS (Gap%). Methods are ordered by J_{med} within each block.

DGP	λ	Method	J_{med}	J_{SD}	$J_{Q_{25}}$	$J_{Q_{75}}$	EC_{med}	Gap%
DGP1	0.50	GP-BO	147,284	25,438	131,164	167,370	41,823	-0.71
		ACFS	148,344	13,811	138,512	158,360	42,448	0.00
		CEM-SO	148,872	22,634	140,675	160,646	42,867	+0.36
		SGD-CVaR	175,178	57,814	149,515	205,946	48,680	+18.09
	KDE-SO	217,294	198,869	179,667	316,872	60,285	+46.48	
	0.70	GP-BO	178,842	38,294	165,930	204,661	40,416	-2.62
		ACFS	183,661	20,479	171,653	195,270	41,419	0.00
		CEM-SO	195,800	32,179	179,048	214,192	42,925	+6.61
		SGD-CVaR	212,139	178,980	184,858	258,101	46,773	+15.51
	KDE-SO	266,973	237,362	207,687	352,867	56,849	+45.36	
	0.90	ACFS	223,405	34,674	210,751	241,645	41,508	0.00
		GP-BO	225,628	65,961	199,301	256,274	41,298	+1.00
CEM-SO		243,081	34,714	224,179	270,397	43,709	+8.81	
SGD-CVaR		261,606	127,013	235,951	318,496	47,152	+17.10	
KDE-SO	324,096	257,886	253,487	447,789	55,017	+45.07		
DGP2	0.50	ACFS	268,105	32,497	244,067	283,904	56,286	0.00
		CEM-SO	308,239	43,238	282,700	331,118	76,358	+14.97
		GP-BO	321,585	63,980	272,640	356,394	104,730	+19.95
		SGD-CVaR	378,008	274,958	330,029	429,505	113,287	+40.99
	KDE-SO	432,431	925,061	363,248	599,130	123,502	+61.29	
	0.70	ACFS	349,167	43,925	323,798	372,513	55,830	0.00
		GP-BO	370,213	72,320	335,051	431,092	102,453	+6.03
		CEM-SO	398,135	60,689	371,593	446,322	77,695	+14.02
		SGD-CVaR	469,846	123,283	414,031	569,792	109,385	+34.56
	KDE-SO	580,007	981,140	496,424	809,847	126,932	+66.11	
	0.90	ACFS	417,761	58,634	388,204	454,644	54,926	0.00
		GP-BO	466,859	108,800	412,926	560,931	106,460	+11.75
CEM-SO		482,813	78,704	452,660	524,966	78,817	+15.57	
SGD-CVaR		569,724	188,902	492,214	663,633	107,548	+36.38	
KDE-SO	716,947	1,890,284	573,802	863,065	128,242	+71.62		

Table 8

Hyperparameter sensitivity analysis on DGP1, $\lambda = 0.70$, $\alpha = 0.95$; 20 replications per grid point. Each parameter is varied independently while others are held at their defaults (shown in bold). J_{med} and J_{SD} are the median and standard deviation of oracle spectral risk across replications.

Parameter	Value	J_{med}	J_{SD}	$J_{Q_{25}}-J_{Q_{75}}$
N_A (LHC size)	800	196,737	30,851	179,735–208,328
	1,200	186,899	21,778	174,971–213,603
	1,600	183,572	37,785	164,612–195,105
n_f (GRF re-rank MC)	400	186,955	17,689	172,255–201,228
	800	190,667	17,707	177,589–203,988
	1,200	182,906	23,887	171,159–205,415
K (elite centres)	2	190,692	25,637	177,155–205,795
	4	193,682	32,905	180,724–211,081
	6	186,780	22,103	177,966–199,518
n_d (direct-DGP MC)	300	188,280	37,535	172,216–202,039
	450	187,773	46,132	174,159–208,195
	600	172,427	23,851	163,785–187,496